Journal of Geodynamics 158 (2023) 102002

Contents lists available at ScienceDirect

Journal of Geodynamics

journal homepage: www.elsevier.com/locate/jog

Velocity anisotropy measured on the spherical specimens: History and applications

M. Petružálek [a,*], T. Lokajíček [a], R. Přikryl [c], V. Vavryčuk [a,b]

[a] Institute of Geology of the Czech Academy of Sciences, Prague, Czech Republic
[b] Institute of Geophysics of the Czech Academy of Sciences, Prague, Czech Republic
[c] Institute of Geochemistry, Mineralogy and Mineral Resources, Faculty of Science, Charles University in Prague, Czech Republic

ARTICLE INFO

Keywords:
Ultrasonic velocity anisotropy
Attenuation
Stiffness tensor
Pressure loading
Fabric
Microcrack alignment
Up to 6

ABSTRACT

The anisotropy of elastic properties, including seismic velocities, has already been investigated in the lab over past seven decades. Here, we present a review related to the development of a unique apparatus for the detailed measurement of seismic velocity anisotropy. Its originality lies in measuring velocities on spherical specimens, which allows for determination of the velocity anisotropy as a function of confining pressure loading with high resolution. The 132 directions, covering the sphere in a regular 15° net of meridians and parallels, have proven to be optimal with respect to common heterogeneities of investigated rocks. The device was designed and the first measurements were performed by a research team of the Institute of Geophysics in Prague (Babuška, Pros and Klíma) in 1968, shortly following many pioneer velocity anisotropy studies. Since then, almost 100 papers have been published using the velocity anisotropy measured with this unique device. The review consists of three separate but mutually interconnected parts: (i) historical development; (ii) microstructural insights from an ultrasonic velocity measurement perspective; (iii) macroscale applications to practical problems in geophysics, structural geology and rock mechanics.

1. Introduction

Our understanding of the Earth's interior and its material composition is primarily based on a few physical parameters directly measured by geophysical methods (Fountain and Christensen, 1989; Rudnick and Fountain, 1995; Mussett and Khan, 2000). Among these, measurements of seismic velocity and its anisotropy dominate, as they provide reliable and extensive data compared to other geophysical methods (Babuška and Cara, 1991; Holbrook et al. 1992; Christensen and Mooney, 1995). The data contain information not only about the elasticity and elastic anisotropy of rock-forming constituents – minerals, but also about the presence and nature of voids such as pores and (micro) cracks. However, the data also reflect other complexities such as variations in composition and/or rock fabric, often recognized as seismic reflectors, variable fluid content, brittle/ductile transitions, and the presence of partially molten material (Babuška and Plomerová, 1992; Plomerová et al., 2007; Li et al., 2003). Additionally, in situ seismic wave velocity is influenced by stress/temperature conditions (e.g., Khazanehdari et al., 2000), which, combined with the effects of anisotropy and heterogeneity, make the interpretation of velocity measurements quite complex. Consequently, constructing seismic models for widely defined lithotypes and interpreting field data with a high degree of precision becomes an extremely challenging task.

To enhance the reliability of using field seismic data, laboratory measurement of dynamic elastic properties (preferably P- and S-wave velocities) are of utmost importance. The laboratory approach can simulate the temperature/stress conditions (e.g., Kern, 1978) and also provides direct insights into the structure of the measured rock samples (Almqvist and Mainprice, 2017). This approach facilitates the establishment of links between the effective seismic properties and the rock mineral composition as well as its preferential orientation (Siegesmund et al., 1996; Weiss et al., 1999; Almqvist and Mainprice, 2017). After recognition of the impact of anisotropic rock fabric on the variation in the velocity of elastic waves along principal finite strain ellipsoid axes (e.g., McKenzie, 1979; Ribe (1992), the need for multidirectional measurements becomes evident.

This review is part of a special issue dedicated to the scientific contributions of the eminent researcher Dr. Vladislav Babuška, whose primary focus was seismic anisotropy at all scales, ranging from laboratory experiments to studies of the local, regional, and global Earth's structure

* Corresppnding author.
E-mail address: petruzalek@gli.cas.cz (M. Petružálek).

https://doi.org/10.1016/j.jog.2023.102002
Received 31 March 2023; Received in revised form 9 October 2023; Accepted 11 October 2023
Available online 13 October 2023
0264-3707/

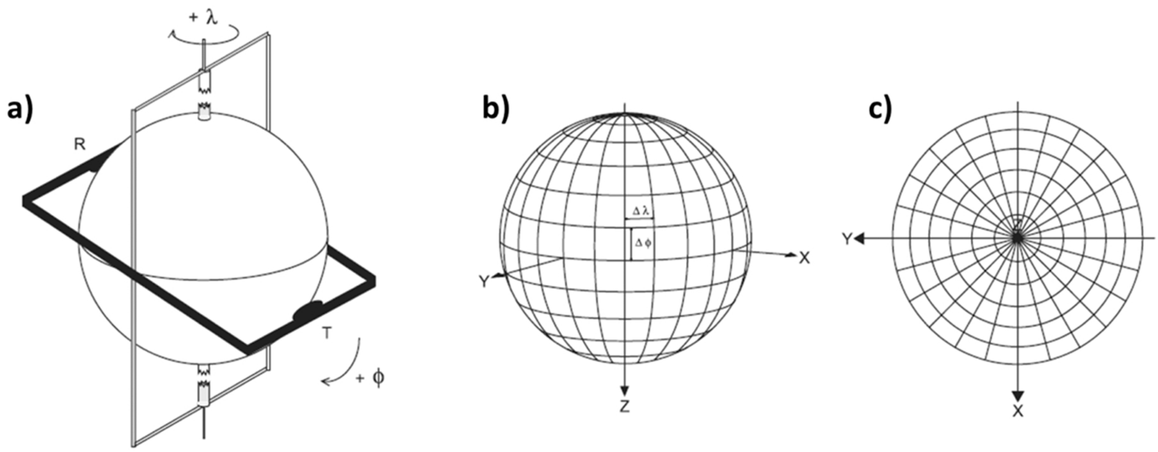

Fig. 1. (a) The experimental design of the measurement on the spherical specimens. (b) and (c) the grids of meridians and parallels used for the measurement (according to Pros and Babuška, 1968, from Pros et al., 1998).

(Babuška and Carra, 1991). Regarding laboratory experiments, his initial works date back to the 1960 s, when he pioneered measurements of seismic anisotropy on spherical specimens at atmospheric pressure (Pros and Babuška, 1967, 1968; Babuška, 1968). Subsequently, this concept was further developed, leading to the design of a worldwide unique experimental apparatus for measuring the pressure dependency of seismic anisotropy (Pros and Podroužková, 1974). While other apparatuses were designed to measure anisotropy on spherical specimens (Thill et al., 1969; Arts et al., 1996), the majority of experimental work was conducted using the Pros and Podroužková (1974) design, or more recently, its direct modification (Lokajíček and Svitek, 2015). Here, we review the development and application of this unique apparatus, which in its final stage of development enables the estimation of pressure-dependent elastic anisotropy in the most general triclinic form involving 21 independent elastic constants (Svitek et al., 2014).

The review is segmented into three sections: (1) theoretical and experimental advancements; (2) microscale applications of anisotropy measurements; and (3) macroscale (in-situ) applications. In each section, a number of exemplary studies were chosen to illustrate the general observations.

2. Velocity anisotropy measured on a spherical specimen

In this section, we describe the history and ongoing development of the pressure vessel for measuring velocity anisotropy on spherical rock specimens. Simultaneously, theoretical advancements were being made as the level of experimental information increased.

The development of a high-precision oscilloscope was a key step for reliable experimental measurements of seismic velocities of ultrasonic pulses detected by piezo-ceramic transducers (Bancroft, 1940). The velocity/pressure and velocity/temperature relations, most interesting for geophysics, have been experimentally studied since ~1950 s (e.g., Hughes and Maurette, 1956 and 1957; Birch, 1960; Christensen, 1965, 1966 and 1979). A typical velocity increase with pressure, related to the microcrack closure, was found for both sedimentary (e.g., Freund, 1992) and crystalline (e.g., Christensen, 1965, 1966) rocks. Simultaneously, a directional dependency of seismic velocity (Christensen, 1965) and its relation to the rock structure (e.g., Brace, 1965) or oriented stresses (e.g., Nur and Simmons, 1969) was recognized and studied.

The original experimental procedure was mostly based on measuring the velocity in three mutually perpendicular directions (Birch, 1960; Christensen, 1965; Lo et al., 1986) often corresponding to already estimated symmetry axes of finite strain ellipsoid (e.g., metamorphic or magmatic foliation and lineation). Typically, cubic, prismatic or cylindrical specimens were used. For example, Kern (1978) described velocity anisotropy variations with pressure (up to 600 MPa) and temperature (up to 700 °C). Characteristically, low-pressure anisotropy (crack-related, extrinsic) is very high (15–30%), and it exponentially decreases with applied pressure (Birch, 1960; Christensen, 1965). When the cracks are closed, the remaining anisotropy is practically pressure independent and attributed to the rock matrix (2–15%, intrinsic; Birch, 1960; Christensen, 1965). The threshold for crack-closing pressure is expected to be in the range of 150–500 MPa for most rocks (Greenfield and Graham, 1996). However, for mantle rocks, Christensen (1974) suggested the influence of rock properties by cracks up to 1000 MPa. The geometry of the microcracks has strong influence on the crack closure, as is outlined in Walsh (1965), Berg (1965), and Mavko and Nur (1978) for different 2D crack shapes.

While anisotropy estimation from three mutuality perpendicular directions yielded valuable results (Birch, 1960; Christensen, 1965; Lo et al., 1986), it also presented weak points: (1) knowledge of the orientation of principal symmetry axes is necessary for designing the experiment; (2) this orientation should not change with pressure due to crack closure (Lokajíček et al., 2021); and (3) the measurement is sensitive to the presence of heterogeneities in any of the three given experimental directions. Moreover, if velocities are measured only in the directions of the symmetry axes, a direct estimation of anisotropic elastic constants is not possible even for the simplest case of transverse isotropy (see e.g., Sarout et al., 2007). To overcome the aforementioned limitations, polyhedron (26 or 18 sided) specimens can be used instead of cylinders or cubes (Babuška, 1965, 1968; Arts, 1993). While these experiments were relatively easy to perform under atmospheric pressure, measuring pressure dependencies proved much more challenging. A significant number of transducers and related electronics needed to be placed in a specially designed pressure vessel. Coating a polyhedron specimen to isolate the rock specimen from the confining fluid was also complicated. When P- and S-wave velocities were measured, repetitive measurements for each wave phase were required (Sano et al., 1992).

Pros and Babuška (1968) and Babuška (1968) tested successfully an apparatus for measuring the velocity anisotropy on a spherical specimen under atmospheric conditions. A similar approach was described by Thill et al. (1969). Simultaneously, Vickers and Richard (1969) suggested a procedure for reliable manufacturing of precise spherical specimens. From the experimental point of view, the main advantage of the sphere was usage of just a single pair of P-wave transducers. The combined effect of rotations of the sphere itself and the transducer pair allowed a practically unlimited number of measurement directions (Fig. 1a). However, 132 directions have been selected to measure the velocity anisotropy in a regular 15° grid of meridians and parallels (Fig. 1b,c).

Later on, Pros and Podroužková (1974) developed the pressure vessel containing the above-mentioned apparatus, which allowed the

Table 1
Research teams and institutes related to the experimental measurement of elastic wave velocity anisotropy on a spherical specimens. IGF: Institute of Geophysics of the Czech Academy of Science, Prague, Czech Republic. IRSM: Institute of Rock Structure and Mechanics of the Czech Academy of Sciences, Prague, Czech Republic. IG: Institute of Geology of the Czech Academy of Sciences, Prague, Czech Republic. MNR: Twin Cities Mining Research Center, Bureau of Mines, Twin Cities, Minnesota, USA. IFP: Geophysics Department, Institut Francais du Petrole, Rueil Malmaison, France. GZG: Geoscience Center, University of Gottingen, Gottingen, Germany.

INST.	Activity	Experimental conditions	Team	# of papers	Cooperation	Exemplary references
IGF	1968–1972	atmospheric pressure, P waves, 132 directions	Pros, Babuška,	~ 10	-	Pros and Babuška, 1967;Babuška et al., 1978
IGF	1974–2000	pressure up to 400 MPa, P waves, 132 directions	Pros, Babuška, Klíma, Lokají ček, Přikryl	~ 30	GZG	Pros and Podroužková, 1974;Pros et al., 1998
IGF	2000–2022	pressure up to 400 MPa, P waves, 132 directions	Machek, Staněk	~ 10	ISRM, IG	Machek et al., 2007;Staněk et al., 2013
IRSM	2000–2006	pressure up to 400 MPa, P, S1 and S2 waves, 132 directions	Lokají ček, Pros, Přikryl	~ 10	IGF, IG	Pros et al., 2003;Přikryl et al., 2007
IG	2006–2023	pressure up to 400 MPa, P, S1 and S2 waves, 132 directions	Lokají ček, Svitek, Petružálek, Vavryčuk	~ 30	IGF, ISRM	Svitek et al., 2014, 2017;Lokajíček et al., 2021
MNR	1969–1973	atmospheric pressure, P waves, 73 directions, possible sample saturation	Thill, Bur, Vickers	~ 5	-	Thill et al., 1969;Thill et al., 1973
IFP	1991–2002	pressure up to 100 MPa, P waves, 144 directions, pore pressure control	Arts, Rasolofasaon	~ 10	GZG	Arts et al., 1996;Rasolofosaon et al., 2002
GZG	1998–2010	pressure up to 200 MPa, P waves, 132 directions	Siegesmund, Weiss	~ 10	IGF, GZG	Ullemeyer et al., 2006; Weiss et al., 2002

anisotropy/pressure relation to be studied in detail (Babuška et al., 1977; Babuška et al., 1984). The differences between low-pressure (cracks, extrinsic) and high-pressure (rock fabric, intrinsic) anisotropy allowed for linking the rock's effective properties with its microstructure (e.g., Babuška and Pros, 1984; Siegesmund et al., 1993). Similar observations can be made while comparing the anisotropy experiments performed on the dried and saturated specimens (Thill et al., 1973; Arts, 1993).

In 1990 s (see Table 1), two more pressure vessels were built allowing for measuring anisotropy on the spheres. Based on their mutual cooperation (Siegesmund et al., 1993, Jahns et al., 1994), the vessel according to the design of Pros and Podroužková (1974) was built at the University of Gottingen. Contrary to the original one (400 MPa), it had lower maximum confinement at 200 MPa (e.g., Ullemeyer et al., 2006). A different design, with a single rotation axis (azimuthal) but 4 pairs of transducers at a fixed azimuthal position (Fig. 2c) was built in the Institut Francais du Petrole (e.g., Arts, 1993; 1996). It allowed for measuring larger spheres (up to the 70 mm), and the maximum confining pressure was 100 MPa; specimens could be saturated and pore pressure controlled.

The brand-new experimental design (Pros 1968; Pros and Babuška, 1968) for measuring elastic wave velocity anisotropy in a dense grid of directions required the development of new methods of inverting the multi-directional measurements for anisotropy parameters. This was done in a pioneering work by Klíma (1973), who proposed an inversion method for estimating a full tensor of 21 independent elastic constants (stiffness tensor) describing general triclinic anisotropy. Linearizing the Christoffel equation, Klíma (1973) suggested an iterative inversion scheme applicable to measurements of the P-wave velocities only or both the P- and S-wave velocities. He found that, when inverting just the P-wave velocities, only 15 P-wave related constants can be obtained reliably. Later on, the essentially same approach, also referred to as the 'weak-anisotropy approximation', was applied by other authors, not only to computing phase velocities but also polarizations, group velocities, ray vectors or travel times of waves in homogeneous as well as inhomogeneous elastic anisotropy (e.g., Cerveny, 1982; Cerveny and Jech, 1982; Thomsen, 1986; Jech and Pšenčík, 1989; Jech, 1991; Gakewski and Psencik (1998); Pšenčík and Vavryčuk, 2002). Once the stiffness tensor is obtained from velocity measurements using the inversion method of Klíma (1973) or others, it can be used to calculate the distribution of the P-wave velocity on the sphere. Such distribution is smooth and less sensitive to heterogeneities and experimental errors than the originally measured data. For this reason, calculated velocities are mostly interpreted instead of the experimentally measured ones (see Fig. 4)..

The multi-directional experimental setup for measuring general triclinic anisotropy posed another theoretical goal: to develop methods for recognizing whether the measured rock sample is truly triclinic or displays some anisotropy symmetry. This problem was first addressed by Klíma et al., (1981), who presented a procedure for finding angles of orthorhombic or higher anisotropy symmetries close to general triclinic anisotropy and for evaluating elastic parameters in the natural anisotropy coordinate system. This procedure became particularly important in mineralogical, geological, and tectonic interpretations of measured rock samples. The procedure was later reinvented or improved by Cowin and Mehrabadi (1987); Baerheim (1993); Bona et al. (2004); Diner et al. (2011); Zou et al. (2013); Aminzadeh et al. (2022), and others.

Pros et al. (1998) used a four-parameter empirical approximation to characterize the velocity/pressure dependency, allowing them to parametrize the intrinsic and extrinsic anisotropy separately. While there were other similar approximations, this one had an intuitive physical meaning. The estimation of these four parameters in 132 independent directions (see Fig. 6b) allowed crack and rock matrix properties to be studied separately and independently in great detail (e.g., Přikryl et al., 2007).

In the year 2000, the original research team led by Dr. Pros, Dr. Klíma, and Dr. Lokajíček moved to the IRSM (see Table 1), while the structural geology group continued to use the original setup for their research at IGF (Baratoux, 2004; Machek et al., 2007; Louis et al., (2012); Staněk et al., 2013). In the following years, a new pressure vessel was designed, developed, and tested at ISRM. Two-step engines were directly included in the pressure chamber. They enabled the automatic control of rotation in two directions: (i) rotation of the sphere around its vertical axis, allowing changes in azimuth; (ii) rotation of the pair of the P-wave transducers around the horizontal axis, allowing variable inclination. Such development, combined with automatic digital recording of waveforms, reduced the experimental time required for a measurement at each pressure step from ~4 h to ~30 min. Moreover, the reliability of experiments increased due to practical elimination human-related errors. As a result, the automation allowed more detailed and more reliable measurements of velocity anisotropy.

Technically, the most challenging task in designing the apparatus was to include a simultaneous measurement of shear waves. The necessity of establishing very good contact conditions for the S-wave transducers was solved by adding a third-step engine that controlled the opening and closing of the arms, in which the sensors were embedded (Fig. 2b). After realizing this improvement by Lokajíček and Svitek (2015), simultaneous measurements of the P-wave and two

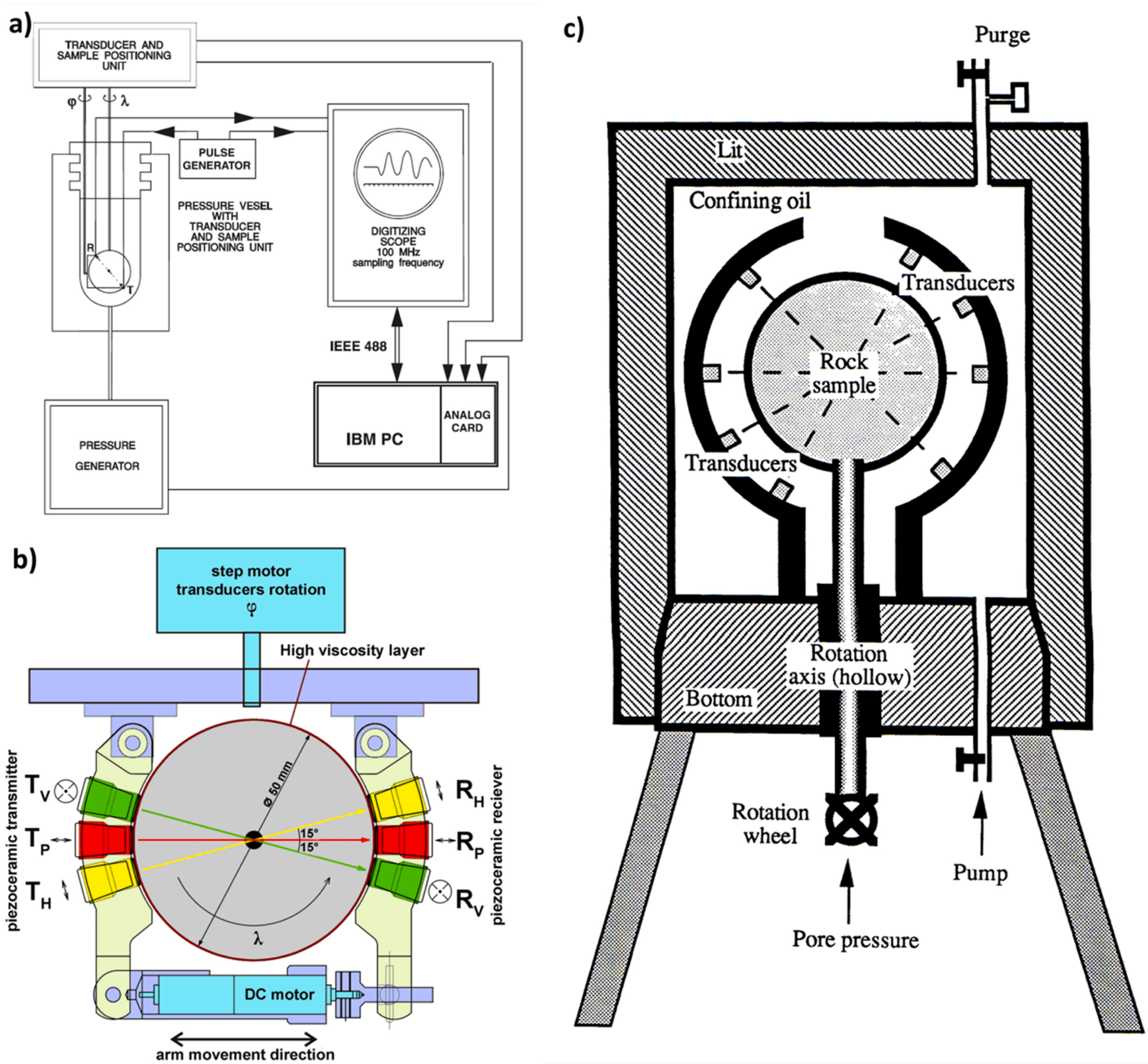

Fig. 2. (a) The experimental setup of an automatic measurement with full waveform recording (Pros et al., 1998); (b) The measuring head designed for simultaneous recording of P-, S1- and S2-wave traces (Lokajíček and Svitek, 2015). (c) The design for measurements of spherical specimen anisotropy at the IFP: Geophysics Department, Institut Francais du Petrole, Rueil Malmaison, France (from Arts et al., 1993).

polarizations of the S-wave are possible (Fig. 2b). While the P-wave onsets can be picked automatically from the seismograms (Lokajíček and Klima (2006); Svitek et al., 2010), a careful manual estimation of the S-wave arrivals is needed (Fig. 3).

The simultaneous measurement of all three wave phases (P, S1, S2), as presented by Svitek et al. (2014), allowed for the first time to estimate the most general stiffness tensor (21 independent elastic constants) using the pulse-transmission method. Moreover, the authors improved the inversion technique for anisotropy parameters by applying a two-step procedure: first, the phase velocities were recalculated from ray (group) velocities measured on the grid of directions, and second, the phase velocities were inverted for anisotropy parameters using the Christoffel equation. In this way, the method is capable of extending the range of anisotropy levels of rocks. The anisotropic velocity distributions of all three phases, based on the input into the inversion, are plotted in Fig. 4. A simplified approach was presented by Pšenčík et al. (2018), who assumed a weak-anisotropy approximation and proposed a linear (non-iterative) method for estimating the full stiffness tensor when the P and S wave velocities are inverted separately.

Recently, a method for identifying higher symmetries in this general stiffness tensor was further developed and successfully tested (Aminzadeh et al., 2022). Table 2 displays low-pressure (0.1 MPa) and high-pressure (100 MPa) stiffness parameters rotated into the orientation of the orthorhombic principal axes. At 100 MPa, the elastic constants are controlled only by the rock matrix. The Bukov gneiss is orthorhombic, while the Grimsel granite practically isotropic. At 0.1 MPa, due to the fully open cracks, there is a decrease in elastic constants by 20–80%. The microcrack alignment resulted in transverse isotropy in the Grimsel granite. The Bukov gneiss remained orthorhombic, but the cracks, aligned with the foliation, significantly increased the level of anisotropy. For both samples, no changes in symmetry orientation related to the increasing pressure were found

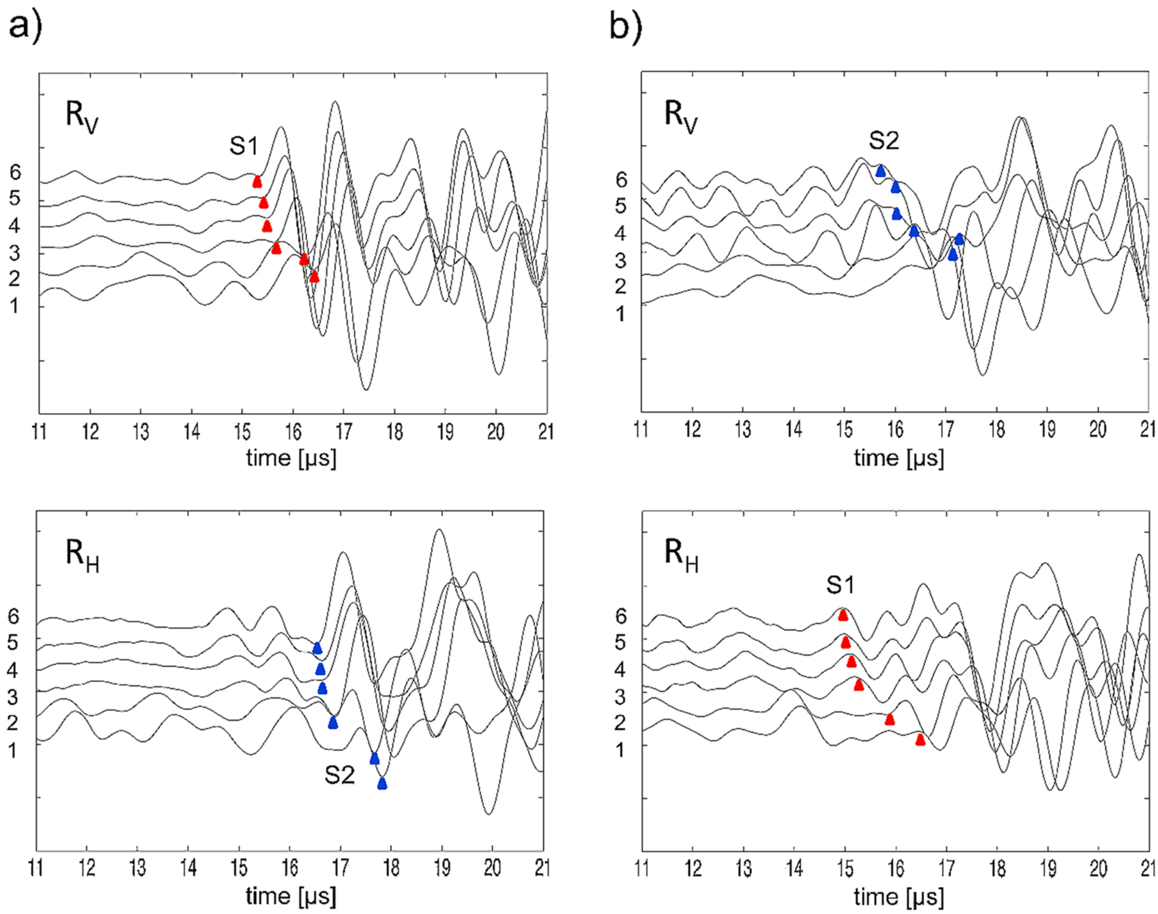

Fig. 3. Examples of waveforms of ultrasonic signals observed for the OKU-409 sample on the transverse receivers: (a) waveforms in a direction in which clear S-wave onsets are observed, (b) waveforms in a direction in which rather unclear and disturbed S-wave onsets are observed. From 1–6, the pressure level is increasing: 0.1, 5, 10, 20, 40 and 70 MPa. From Svitek et al. (2014).

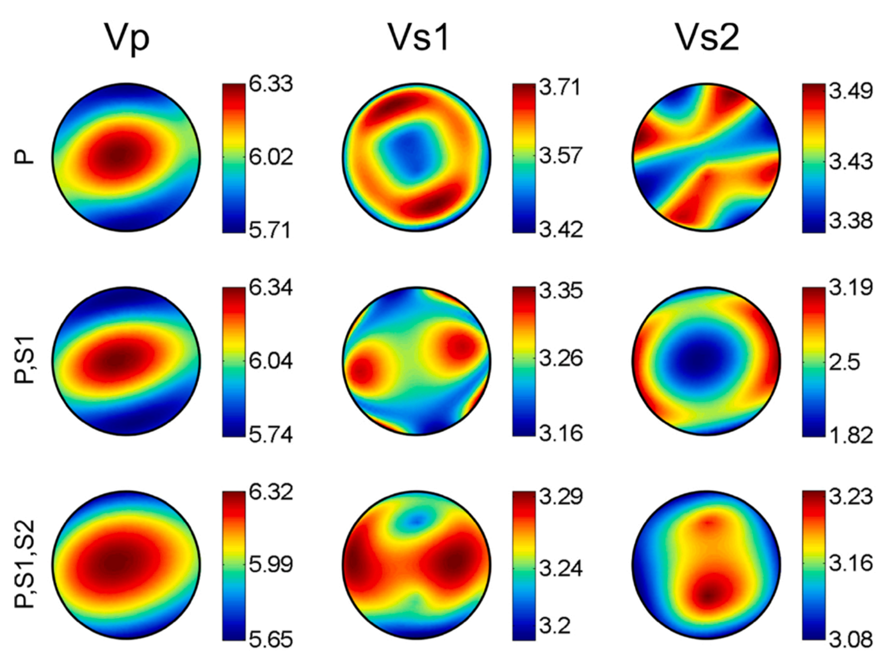

Fig. 4. Phase velocities of the P (left-hand column), S1 (middle column) and S2 (right-hand column) waves corresponding to the elastic parameters retrieved by inverting three different data sets: the P-wave velocities only (top row), the P- and S1-wave velocities (middle row), and the P-, S1- and S2-wave velocities (bottom row). The confining pressure is 70 MPa. From Svitek et al. (2014).

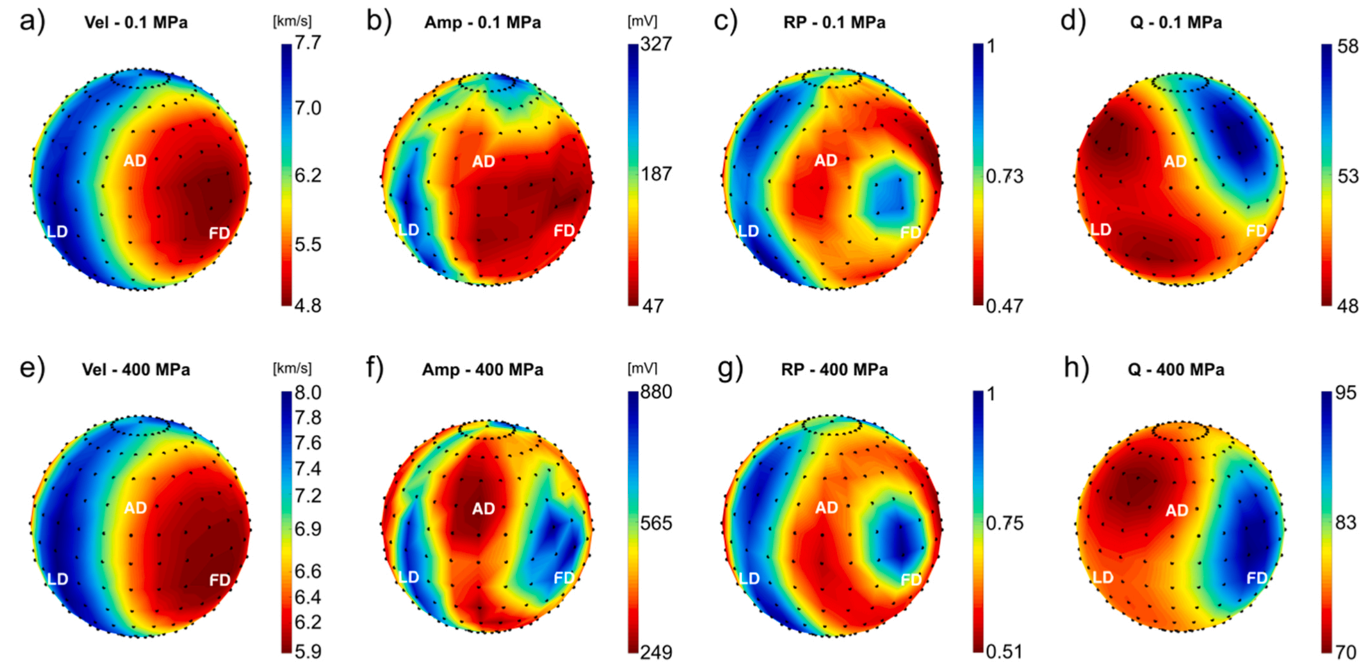

Fig. 5. The 3D projection on spherical surface of measured velocities (a,e), amplitudes (b,f), calculated normalized radiation pattern (RP) (c,g) and ray *Q*-factors (d, h) at 0.1 and 400 MPa, respectively. The black dots represent points of measurement and the white letters mark the selected directions – lineation (LD), foliation normal (FN) and amplitude minimum (AD). The positions of the LD, FN and AD directions are marked by the circle, cross and plus sign, respectively. The x_1, x_2 and x_3 axes show the orientation of the sample. View point (−40°, 20°). After Svitek et al. (2017).

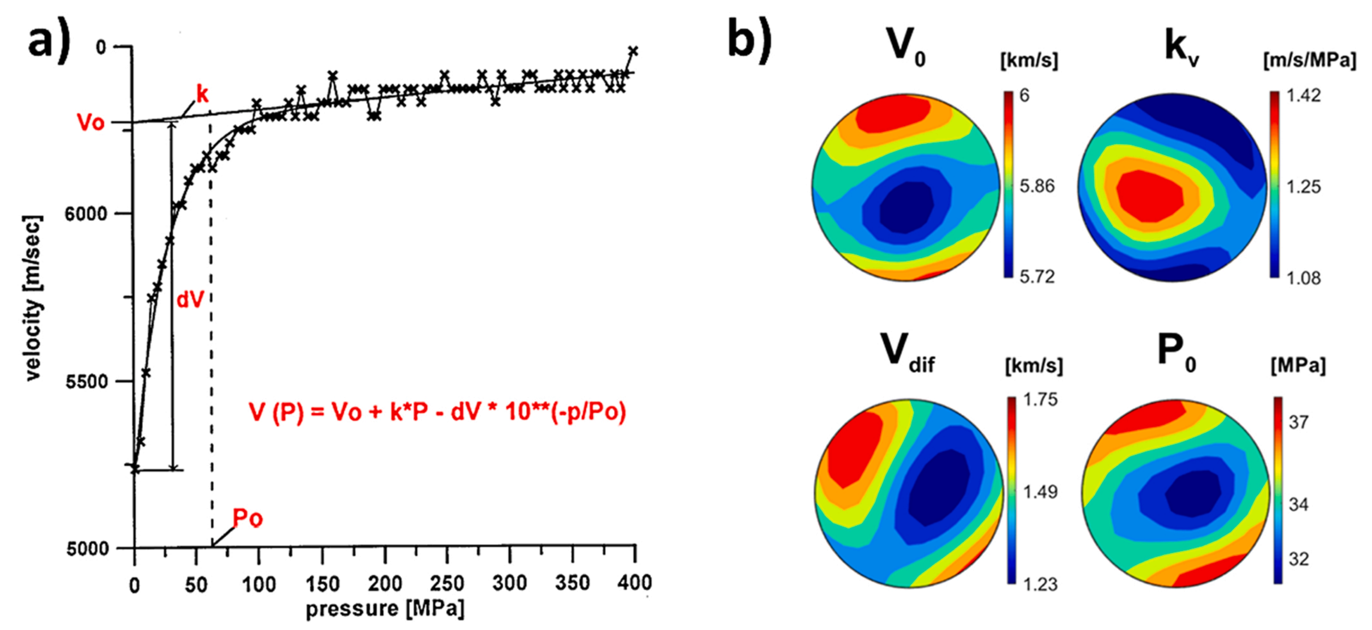

Fig. 6. (a) Nolinear velocity/pressure approximation and its four parameters (Pros et al., 1998). The four parameters in the equation are explain in the text. (b) The anisotropic distributions of four parameters form a non-linear approximation. Measured on the Westerly granite specimen, adjusted according to Lokajíček et al. (2021).

(Aminzadeh et al., 2022).

While velocity anisotropy has been thoroughly studied in the past six decades, studies of seismic attenuation and its anisotropy are rather scarce (e.g., Klíma et al., 1962, 1964; Kern et al., 1997; Jackson et al., 2002; Stanchits et al. 2003). This may be related to significantly higher errors in measured amplitudes when compared to the arrival time picking. In addition, measurements in a few directions strongly limited interpretations of anisotropic attenuation. However, the setup with 132 measurement directions in the sphere experiments allowed mitigating this uncertainty. The problem of determining anisotropic attenuation is also involved from a theoretical point of view. A model of viscoelastic anisotropy must be considered when stiffness parameters of rocks become complex-valued and frequency dependent (Auld, 1973; Carcione, 2014; Cerveny and Psencik (2005); Zhu and Tsvankin, 2006; Vavryčuk, 2007a,b). Moreover, discriminating between phase and ray (group) quantities are even more significant and cannot be neglected (Vavryčuk 2007b, 2015). Based on the above-mentioned theoretical analysis of anisotropic attenuation, Vavryčuk et al. (2017) described an

Table 2
The stiffness tensors [GPa] in its in principal coordinate system for two samples collected at the underground research laboratories. Upper row: Bukov gneiss (Czech Republic), bottom row: Grimsel granite (Switzerland). Left column: atmospheric pressure, right column: measured at 100 MPa. Bolded are the non-zero elastic constants in orthorhombic symmetry. According to Aminzadeh et al. (2022).

$$\begin{bmatrix} \mathbf{90.18} & \mathit{26.30} & \mathit{13.98} & -0.79 & 0.71 & 0.23 \\ & \mathbf{79.09} & \mathit{17.96} & -0.19 & 4.54 & -0.68 \\ & & \mathit{45.03} & 0.91 & 0.91 & -2.81 \\ & & & \mathit{19.33} & 0.45 & -0.97 \\ & & & & \mathbf{22.01} & -0.72 \\ & & & & & \mathbf{28.39} \end{bmatrix} \quad \begin{bmatrix} \mathit{109.32} & \mathit{32.55} & \mathit{33.59} & 0.70 & -1.04 & 0.13 \\ & \mathbf{99.33} & \mathit{37.29} & -1.04 & -3.64 & -0.31 \\ & & \mathit{85.05} & -0.55 & -0.20 & -2.11 \\ & & & \mathit{26.65} & 0.44 & 1.24 \\ & & & & \mathbf{28.66} & 0.42 \\ & & & & & \mathit{35.75} \end{bmatrix}$$

$$\begin{bmatrix} \mathbf{47.09} & \mathit{19.04} & \mathit{11.51} & 0.28 & -0.70 & -0.41 \\ & \mathbf{45.74} & \mathit{12.78} & 0.38 & -2.28 & -1.19 \\ & & \mathbf{23.09} & -0.55 & -0.26 & -1.51 \\ & & & \mathit{8.83} & 1.59 & 0.97 \\ & & & & \mathbf{9.38} & 0.17 \\ & & & & & \mathbf{13.90} \end{bmatrix} \quad \begin{bmatrix} \mathbf{114.82} & \mathit{34.73} & \mathit{33.81} & 1.36 & -0.50 & -0.25 \\ & \mathbf{111.56} & \mathit{36.00} & 0.58 & -1.32 & 0.62 \\ & & \mathit{110.09} & -0.71 & -0.17 & -3.21 \\ & & & \mathit{35.26} & -0.37 & 0.67 \\ & & & & \mathbf{37.39} & 0.13 \\ & & & & & \mathbf{38.49} \end{bmatrix}$$

inversion scheme for calculating parameters of anisotropic attenuation from a directional variation of amplitudes of P- and S-waves. Subsequently, Svitek et al. (2017) applied this inversion for anisotropic attenuation to measurements conducted on a spherical sample of antigorite serpentinite. The authors revealed significant variations of attenuation and the Q-factor with acting hydrostatic pressure (up to 400 MPa) caused mostly by closure of preferentially oriented microcracks. The results proved that knowledge of anisotropic attenuation is essential for understanding rock structure, including the behavior of microcracks.

As is summarized in Table 1, there were eight, mutually interconnected research teams that experimentally measured seismic anisotropy on spheres. As a result, more than 100 scientific papers were published. With the exception of the IFP team (e.g., Arts, 1993; Rasolofosaon and Zinszner, 2002), the rest of them used the original design (Pros and Podroužková, 1974) or its improved modification (Lokajíček and Svitek, 2015). Recently, only the IG team (see Table 1) has been publishing the new anisotropy experimental studies.

Considering future development, a simultaneous measurement of pressure induced sphere deformations looks promising. The anisotropy of static deformation is measured along the sphere's diameter using LVDT in the same 132 independent directions as the seismic velocities. This approach could allow for studying relations between dynamic (seismic waves) and static (deformations) elastic properties.

3. Micro-scale applications

In this section, we will introduce main works obtained through the above-mentioned methodical approaches, which are related to the microscale or petrophysics. Microscale relations refer to the influence of preferential orientations of: (i) crystals (CPO), (ii) mineral grains (SPO) or (iii) micro-crack alignment on the effective anisotropy measured by ultrasonic waves (eg. (Almqvist and Mainprice, 2017). As the later research often serves as a kind of motivation and a source of ideas for future work, this section is ordered chronologically. It provides a historical overview of velocity anisotropy experiments related to rock microstructure, highlighting two interesting examples: (1) Separation of intrinsic and extrinsic anisotropy (Pros et al., 1998), and (2) demonstration of microstructural modelling in comparison with multidirectional measurements of P- and S-wave anisotropy (Vasin et al., 2017).

Birch (1960, 1961) presented a comprehensive velocity anisotropy study (~ 250 specimens), using three specimens drilled in mutually perpendicular directions for each particular rock. Most of the tested rocks were anisotropic at low pressure (due to microcracks), with anisotropy levels decreasing with increasing pressure up to 1000 MPa. At high pressures, only dunites were significantly anisotropic, suggesting a strong CPO of olivine. For metamorphic rocks, Christensen (1965) verified that the minimum velocity direction is perpendicular to their foliation and related the orientation of anisotropy to rock-forming minerals with strong CPOs such as micas, amphiboles, and olivine (Christensen, 1965 and, 1966).

Babuška (1968) stated the necessity of multidirectional experiments to generally verify the anisotropy observations made in preselected orientations. He tested over 150 metamorphic and igneous rocks, shaped as polyhedrons or spheres, under unloaded conditions. The anisotropy was found to be higher for metamorphic rocks, displaying symmetry along the foliation plane. Based on microscopic observations, the link between the CPO of calcite and velocity anisotropy of marble was reported and proven by CPO modelling (Klíma and Babuška, 1968). Using similar multidirectional experiments, Bur et al., (1969) observed orthorhombic symmetry (rhyolite, limestone, granodiorite) or transverse isotropy (shale, marble) as the typical symmetries that can be expected in an unloaded state. Thill et al., (1969) recognized three different sources of anisotropy. As already mentioned, the CPO of calcite was responsible for anisotropy in marble. The SPO of elongated vesicles was related to the anisotropy in Newberry Crater pumice. The aligned cracks in quartz were linked to the anisotropy in granite. These pioneer multidirectional measurements mostly confirmed the already expected relation between rock structure and velocity anisotropy stated in the previous paragraph but were not able to distinguish between crack and fabric related anisotropy.

To separate extrinsic and intrinsic anisotropy, the application of confining pressure was necessary. Babuška (1972) used 13 oriented cylinders to study two mono-mineral lower-crust rocks (dunite and bronzite) and reported a good correlation between of measured high-pressure velocity anisotropy and that calculated from the fabric. Thill et al. (1973) interpreted the velocity differences measured on saturated and dried spherical specimens with respect to fabric or crack preferential orientation. Babuška et al. (1977) found the cleavage cracks in biotite and hornblende to be responsible for strong extrinsic anisotropy in granodiorite, which was practically isotropic at 300 MPa. Babuška and Pros (1984) quantitatively correlated low-pressure anisotropy with the preferential orientation of cracks. In the case of granodiorite, the cleavage-related cracks in biotite and hornblende were found to be responsible for low-pressure anisotropy. By contrast, grain boundary cracks had a higher influence in the basically mono-mineral quartzite with almost random CPO. Siegesmund et al. (1993) related the velocity anisotropy axes (extreme velocity directions) and the macro-structural features (foliation, lineation) of two orthogenesis and by the CPO modelling verified that biotite is the main source of its fabric-related transverse isotropy. Arts et al. (1996) presented an experimental and theoretical approach for separation of extrinsic and intrinsic anisotropy and estimation of the level of symmetry and its orientation. Zang et al. (1996) used an approximation of the

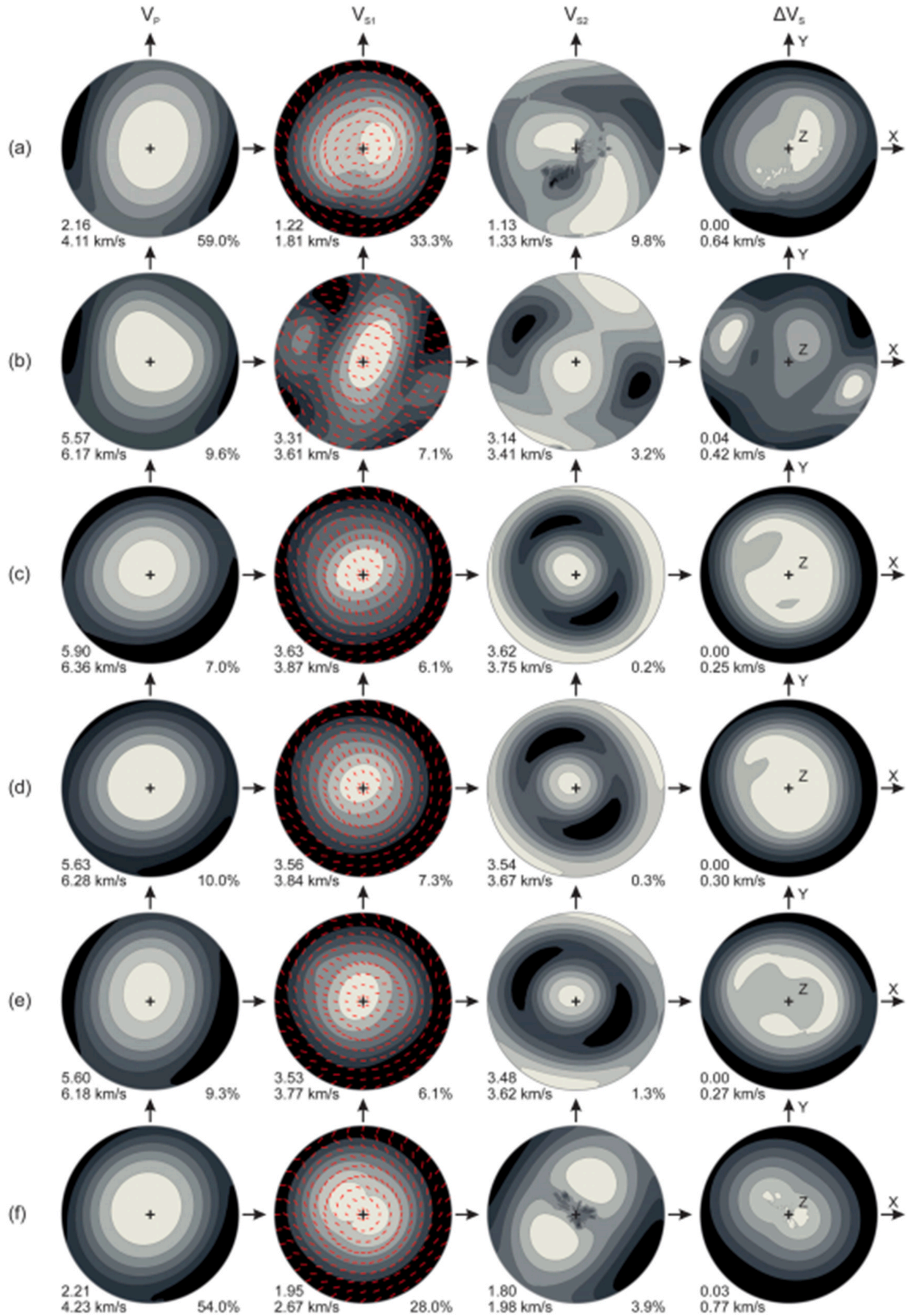

Fig. 7. Group velocity distributions (VP, VS1, VS2) as well as shear wave splitting VS in Tambo gneiss spherical sample during the second experimental run ((a) – at 0.1 MPa and (b) – at 100 MPa pressure) (Fig. 2b, black lines) and different Tambo gneiss models ((c) – without pores and cracks; (d) – with 0.1 vol% of primary cracks; (e) – with 0.1 vol% of primary cracks and 0.6 vol% of secondary cracks (cf. Fig. 2b, red lines); (f) – with 2.6 vol% of primary cracks and 1.0 vol% of secondary cracks). Fast S-wave polarization projections for different wave propagation directions are shown as red dashes on corresponding projections. Minimum and maximum velocity values, as well as A–V anisotropy coefficient are shown. Equal area projections, linear scale contours normalized to the minimum and maximum of each projection (Vasin et al., 2017).

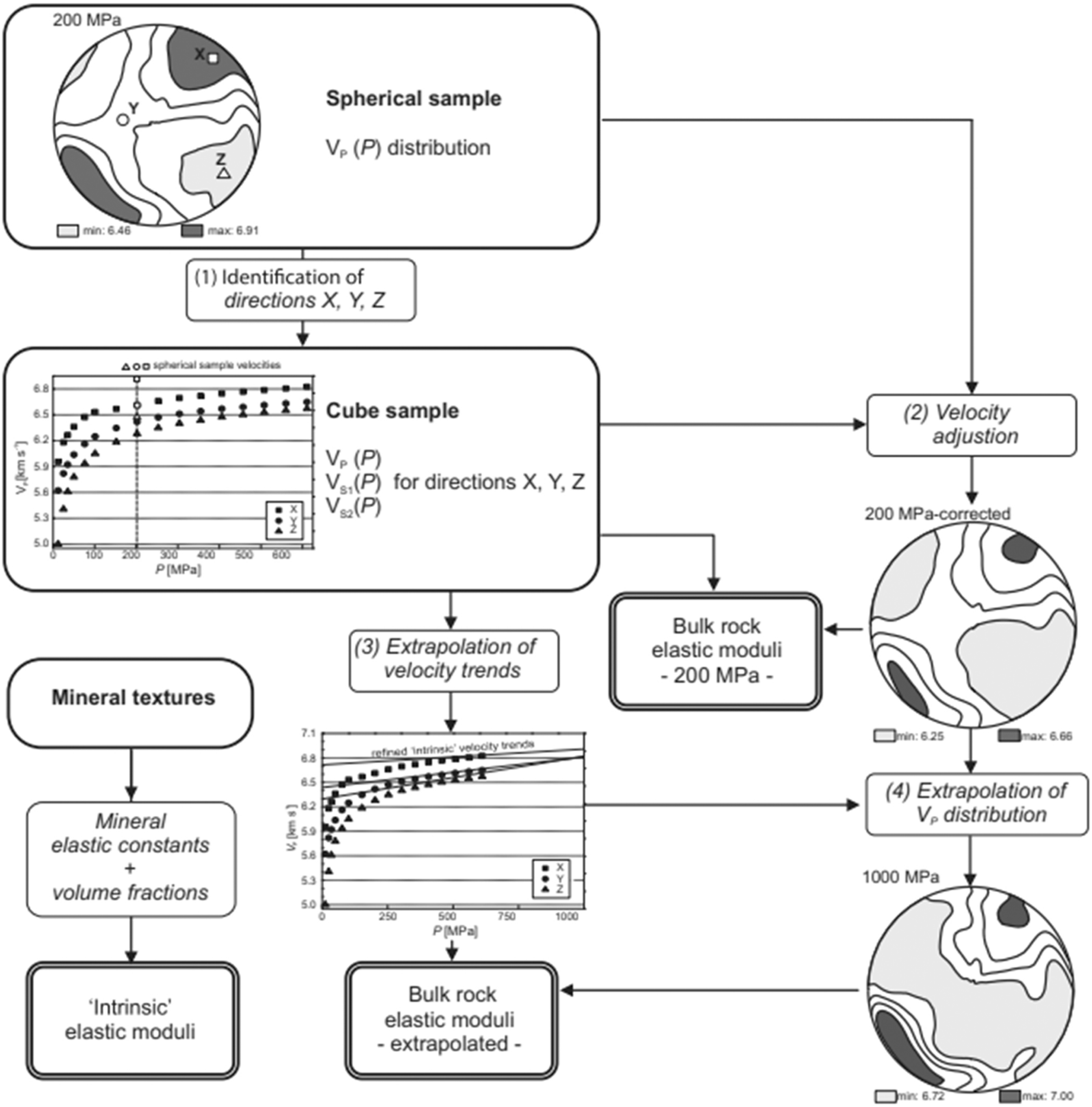

Fig. 8. Workflow scheme using amphibolite sample demonstrating step by step the applied procedures (from Ullemeyer et al., 2018).

velocity/pressure trend to estimate a directionally dependent crack closing pressure and linked the extrinsic velocity anisotropy to the in-situ orientation of horizontal stresses. Rasolofosaon et al. (2000) recognized the transverse isotropy related to the CPO of biotite (Siegesmund et al., 1993) is significantly increased by the presence of biotite-related grain boundary and cleavage cracks at low pressures. Machek et al. (2006) recognized the grain boundary of clinopyroxene and its cleavage cracks are responsible for low pressure anisotropy in eclogite.

On an intuitive level, Pros et al. (1998) suggested a four parameter approximation of the typical velocity/pressure trend (Fig. 6a). This allowed for a separate characterization of intrinsic and extrinsic anisotropy.

Two parameters characterize a linear, crack-free, high-pressure (rock-matrix) dependency: V_0 is the ideal velocity in the crack-free unloaded rock, and k is the linear influence of pressure on the elasticity of the rock matrix. Two parameters described the exponential increase at low pressures attributed to the microcrack closure: dV (V_{dif}) is the difference between the v_0 and the real, measured velocity in an unloaded rock, which is proportional to the amount of open cracks at the unloaded state. P_0 is the pressure at which the dV decreases to the 10% of its original value, related to the crack closing pressure. While several other approximations of velocity/pressure dependency have been proposed and investigated (Zang et al., 1996; Wang et al., (2015); Ji et al., 2007; Ullemeyer et al., 2011; Ullemeyer et al., 2018), the work of Pros et al. (1998) is valuable mainly for its easy and intuitive application. The intrinsic velocity (V_0 in Fig. 6b) of the Westerly granite displays weak anisotropy related to the CPO of feldspars (Lokajíček et al., 2021).

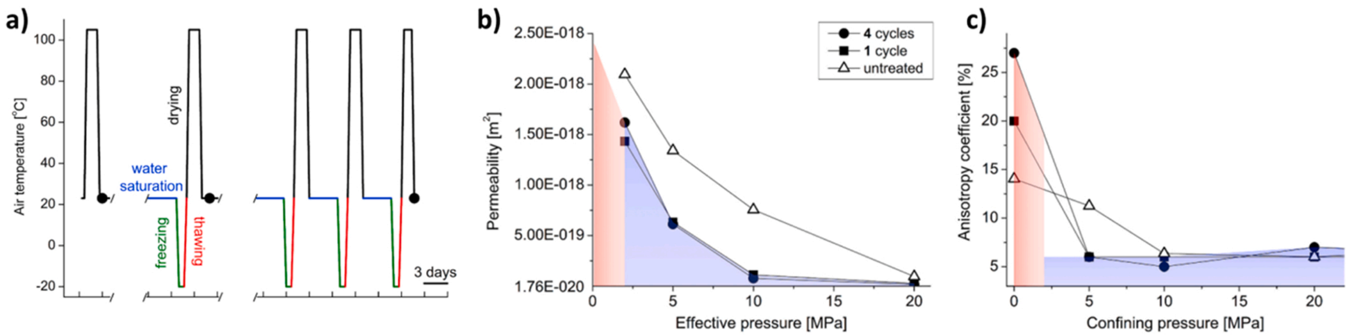

Fig. 9. a) Temperature conditions during rapakivi rock testing. Circles denote measurements of P-wave velocities on a sphere and permeability on the cylinder. The pressure dependence of: (b) water transport properties; (c) the anisotropy coefficient after different cycles of F-T tests. Shadowed areas highlight pressure intervals with the largest (up to 2 MPa) and lowest (above 2 MPa) contribution of cracks with preferred orientation (from Ivankina et al., 2020).

Interestingly, it increases faster in its minimum (lower stiffness) direction (k in Fig. 6b). The size and orthorhombic anisotropy in V_{dif} were related to the microcracks parallel to the cleavage planes of feldspars and biotite (Lokajíček et al., 2021). Only slight anisotropy in P_0 may be related to the rather directionally independent aspect ratio of contained cracks. The anisotropic distribution of these four parameters (Fig. 6b) had often been used in later publications, namely in relation to the CPO/SPO/crack alignment-based calculated velocity anisotropy (e.g., Ullemeyer et al., 2006; Přikryl et al., 2007; Ivankina et al., 2017; Lokajíček et al., 2021).

As already mentioned, the anisotropy/fabric relation has mostly been studied for monomineralic rocks, such as marble, limestone, quartzite, and dunite. Texture measurements made by neutron tomography (Ullemeyer et al., 1998; Wenk et al., 2003) and their processing (Wenk et al., 1998) together with the modeling of elasticity of polyphase rocks (Mainprice and Humbert, 1994; Matthies and Humbert, 1993) present a powerful tool for estimating intrinsic anisotropy (Almqvist and Mainprice, 2017) for polyphaser rocks. High-pressure anisotropy was successfully correlated with the CPO (from neutron diffraction) based models of multiphase crystalline rocks (Kern et al., 2008; Lokajíček et al., 2014; Vasin et al., 2017). Introducing one or two systems of aligned microcracks (as SPO of microcracks) into self-consistent models (GEO-MIX-SELF, Matthies, 2012) significantly improved the fit between measured and modelled velocity anisotropy (Vasin et al., 2017; Ivankina et al., 2020; Keppler et al., 2021) at low pressures. When the crack- and fabric-related anisotropy axes are not parallel, the symmetry axes rotate with increasing pressure due to the micro-crack closure (Lokajíček et al., 2021). Surprisingly, the SPO of isolated mica grains or its layering had only a minor influence on effective anisotropy (Vasin et al., 2017; Ivankina et al., 2017). Following the works of Svitek et al. (2014) and Lokají ček et al. (2015), the joint measurement of P- and S-wave velocity anisotropy has been possible. A reasonably good agreement was found between measured data and texture-based models of elastic anisotropy (Lokajíček et al., 2014; Kern et al., 2015; Vasin et al., 2017). For two samples of biotite gneiss, anisotropy of magnetic susceptibility and P-wave velocity was found to coincide. Based microstructural modelling, the CPO of biotite was main source of anisotropy (Zel et al., 2021).

To demonstrate the comparison of microstructural modelling and the experimentally obtained anisotropy at low and high pressure (Fig. 7) we present an example of the biotitic Tambo gneiss (Vasin et al., 2017). To best fit the low (Fig. 7a) and high (Fig. 7b, 100 MPa) experimental anisotropy, the inclusion of two microcrack systems (Fig. 7e,f) in the microstructure was necessary. The agreement between measured and modelled velocity is very good for P waves, fairly good for shear S1 waves, but significant differences were recognized for the S2 phase. This was reflected in elastic constants. Purely P-wave velocity elastic constants matched very well. However, for those related to the shear waves, the discrepancy between the model and experiment was ranging from 15% to 30% (Vasin et al., 2017).

4. Macro-scale applications

Here, we focus on the practical impact of anisotropy measurements, specifically in rock mechanics, geophysics and structural geology. In previous sections, we described the sources of extrinsic anisotropy (cracks) and intrinsic anisotropy (CPO, SPO) as well as the methods for their separation.

Intrinsic anisotropy is particularly interesting for high-pressure applications, when cracks are closed. This is especially relevant in deep geophysics and structural geology, particularly when considering anisotropic properties in the Earth's crust and upper mantle (Babuška and Cara, 1991). While here we focuse mainly on the experimental anisotropy measurements, it's important to note that the intrinsic anisotropy is mostly obtained from the CPO modelling (Almqvist and Mainprice, 2017).

Pros et al. (2003) examined 11 ultrabasic rocks from Ivrea zone. Most of them displayed only marginal extrinsic anisotropy and the velocity/pressure relation often exhibited linear behavior from the beginning of loading. The high-pressure velocity patterns resembled orthorhombic symmetry or transverse isotropy, with intrinsic anisotropy levels from 5% to 8%. Ullemeyer et al. (2006) characterized the seismic velocity and its anisotropy in 12 different typical metamorphic rocks along the TRANSALP traverse seismic profile. The experimentally determined intrinsic anisotropy ranged from 5% to 15%, while the texture-based modelling displayed significantly lower values. A good match was found just for monomineralic marbles and amphibolite, whereas the difference for polycrystalline rocks it was 5–10%. Martínková et al. (2000) extrapolated the high-pressure (400 MPa) experimental velocities of granite, nephelinite and lherzolite, founding reasonably good agreement with vertical seismic velocity model used for the seismically active area of West Bohemia. Keppler et al. (2015) modelled (CPO) velocity anisotropy from the Eclogite Zone of the Tauern Window and reported reasonably good agreement between velocity anisotropy patterns of amphibolite and eclogite, but a higher level of anisotropy for experimental data. Keppler et al. (2021) explained the differences in experimental and modelled velocities and its anisotropy by the presence of open microcracks even at pressure of 400 MPa. They expected the cracks to be closed at approximately 740 MPa (28 km depth). As can be seen, the main challenge in obtaining reliable intrinsic elasticity from multidirectional measurements is the necessity to exceed the 400 MPa pressure (Ji et al., 2007), where the influence of cracks is marginal enough. Due to the technical limitations, this is currently not feasible for measurements on spherical specimens. An alternative approach was presented by Ullemeyer et al. (2018). They used two anisotropic experimental datasets (sphere and cube) to extrapolate intrinsic elasticity to 1000 MPa (Fig. 8). The extrapolation results were reasonably comparable to the modelled ones.

If we separate the influence of cracks on velocity and its anisotropy (V_{dif} in Fig. 6b), we can gain insight into how they control low-pressure

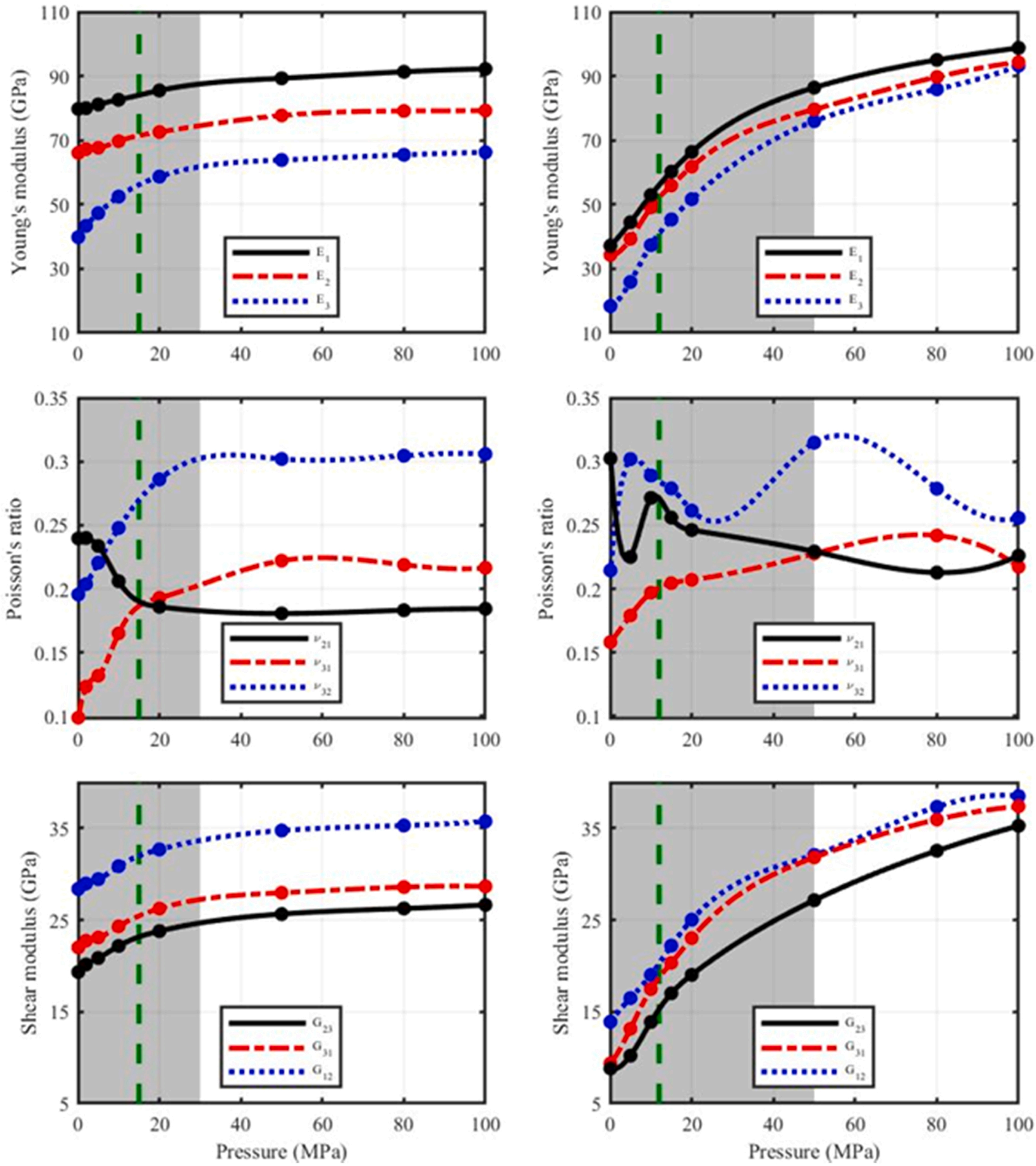

Fig. 10. Elastic parameters ($E_1, E_2, E_3, \nu_{21}, \nu_{31}, \nu_{23}, G_{23}, G_{31}, G_{12}$) in three principal planes for the BUK sample (left) and for the GRM sample (right). The gray interval is dominated by the presence of cracks; the white region is controlled by the rock matrix. The border between both regimes represents a crack-closing pressure. The green dashed line corresponds to the expected lithostatic pressure at the corresponding URLs (from Aminzadeh et al., 2022).

anisotropy. Often, one or two microcrack systems result in transverse isotropy or orthotropic V_{dif} patterns (e.g., Ullemeyer et al., 2006). The V_{dif} patterns can help estimate the orientation of the main crack systems and serve as an input for calibrating microstructure models when cracks are included (e.g., Ivankina et al., 2020). Given that the size of microcrack porosity and its preferential orientation significantly impact the mechanical properties of rocks (e.g., Přikryl et al., 2007), the V_{dif} parameter can be used to estimate rock quality (Weiss et al., 2002) or describe changes related to degradation processes in rock, such as thermal loading (Weiss et al., 2002; Lokajíček et al., 2021) or freeze/-thaw cycling (Ivankina et al., 2020). When cracks are interconnected (Ivankina et al., 2020), microcrack porosity essentially controls intergranular permeability (Rasolofosaon et al., 2002).

As a demonstration of statements in previous paragraph, we provide a more detailed description of the study by Ivankina et al. (2020). The heavily cracked rapakivi granite underwent freeze/thaw cycles (Fig. 9a), and the effects were analyzed through ultrasonic sounding, permeability measurements, and microstructure modelling. Initially, the granite contained three crack systems: random and two aligned ones. Interestingly, only one aligned crack system was interconnected, leading to a step-by-step increase in anisotropy from an initial 15–25% due to freeze/thaw cycles (0 MPa in Fig. 9c). Surprisingly, the measured permeability decreased (Fig. 9b). One possible explanation could be the easier closing of interconnected microcracks, as demonstrated by lower anisotropy (at 5 MPa) after freeze/thaw cycling (Fig. 9c).

The application of combined (extrinsic and intrinsic) anisotropy, due to the high influence of open cracks, has potential in shallow depth, mainly rock mechanics-related problems. However, the recognizable impact of cracks can be traced up to the 300–400 MPa (Keppler et al., 2021). A reasonably good fit between experimental and sonic log velocities (down to 4 km depth) suggests that hydrostatic pressure can simulate the influence of the overburden (e.g., Berckhemer et al., 1997). It is a well-known fact than the fabric can be related to the anisotropy of mechanical properties of rocks (e.g., Shea and Kronenberg, 1993; Rawling et al., 2002; Hakala et al., 2007; Petružálek et al., 2019). Following are two examples of detail anisotropy measurements directly related to the rock mechanics.

Přikryl et al., (2007) measured velocity anisotropy on spheres up 400 MPa on the set of 8 crystalline rocks. The same rocks were uniaxially loaded, and static moduli, together with UCS, were estimated. They recognized that the level of extrinsic anisotropy correlated with the anisotropy of static moduli, while the UCS anisotropy was related more to intrinsic anisotropy. By combining various types of symmetry and orientations of extrinsic and intrinsic anisotropy, they characterized the most common geomechanical models.

Using the P- and S-wave velocity anisotropy measurements, the orthorhombic stiffness tensor can be derived from the triclinic one and expressed using the engineering elastic constants characterizing orthotropy (Aminzadeh et al., 2022): $(E_1, E_2, E_3, \nu_{21}, \nu_{31}, \nu_{23}, G_{23}, G_{31}, G_{12})$. Pressure-dependent elasticity is important in applications related to deep mines or hazardous waste deposits, where the acting lithostatic pressure is significant. Aminzadeh et al., (2022) reported orthotropy for the Bukov gneiss (Czech Republic) and transverse isotropy for the Grimsel granite (Switzerland) at pressures equivalent to the in-situ depths of both underground research laboratories (Fig. 10).

5. Conclusions

The continuous 60 years of development led to a step-by-step improvement of the original experimental apparatus designed to measure velocity anisotropy with unprecedented accuracy under hydrostatic pressure loading on spherical specimens. The main improvement was the simultaneous measurement of three seismic velocity phases (P, S1, S2), each in 132 independent directions. The obtained results enabled the estimation of the stiffness tensor in its most general triclinic form (21 independent constants). When the material displayed higher symmetry, this symmetry was recognized, and the general stiffness was simplified accordingly, such as into transverse isotropy or orthotropy. The pressure loading served as a simulation of lithostatic pressure and allowed to study crack- and fabric-related anisotropy independently. The experimental results proved to have shown a broad range of potential, particularly in the fields of petrophysics, rock mechanics, geophysics, and structural geology.

CRediT authorship contribution statement

Paper: Velocity anisotropy measured on the spherical specimens: history and applications Authors: Petružálek M., Lokajíček T., Přikryl R. and Vavryčuk, V. The mentioned review paper was a joint work of the entire author collective. The corresponding author (Petružálek M.) is responsible for ensuring that the description is accurate and agreed by all authors.

Declaration of Competing Interest

The authors declare that they have no known competing financial interests or personal relationships that could have appeared to influence the work reported in this paper. The corresponding author (Petruzalek M.) is responsible for ensuring that the description is accurate and agreed by all authors.

Data availability

No data was used for the research described in the article.

Acknowledgment

The authors would like to thank their previous colleagues. Without their participation, most of the scientific work presented in this review would have been hardly possible. Ing. Zdeněk Pros designed and constructed the apparatus for measuring seismic wave velocities on spherical specimens. Dr. Karel Klíma developed the theory, algorithms, and codes for the inversion of experimental data into the form of the stiffness tensor. Dr. Vladislav Babuška played a pivotal role in applying the obtained results within the rock structure and geophysical context. We greatly appreciate their work and proudly follow in their footsteps. We are grateful to Bjarne Almqvist and one anonymous reviewer for providing their detailed comments and giving us the opportunity to improve the original manuscript. Considering the funding, the study was partially supported by the Czech Science Foundation research grants CSF 21–26542S and 22- 00580S and by the Czech Academy of Sciences projects RVO 67985831.

References

Almqvist, B.S., Mainprice, D., 2017. Seismic properties and anisotropy of the continental crust: Predictions based on mineral texture and rock microstructure. Rev. Geophys. 55 (2), 367–433.
Aminzadeh, A., Petružálek, M., Vavryčuk, V., Ivankina, T.I., Svitek, T., Petrlíková, A., Lokajíček, T., 2022. Identification of higher symmetry in triclinic stiffness tensor: application to high pressure dependence of elastic anisotropy in deep underground structures. Int. J. Rock. Mech. Min. Sci. 158, 105168.
Arts, R.J., 1993. A study of general anisotropic elasticity in rocks by wave propagation: Theoretical and experimental aspects. Ph.D. thesis, Institut Fran¸cais du Petrole.
Arts, R.J., Rasolofosaon, P.N.J., Zinszner, B., 1996. Experimental and theoretical tools for characterizing anisotropy due to mechanical defects in rocks under varying pore and confining pressures. In: Fjaer, E., Holt, R.M., Rathore, J.S. (Eds.), Seism. anisotropy, Soc. Explor. Geophys. 384–432 (Tulsa).
Auld, B.A., 1973. Acoustic Fields and Waves in Solids. Wiley.
Babuška, V., 1965. Velocity of compressional waves and elastic anisotropy of some igneous and metamorphic rocks. Geofyzikální sborník 275–292.
Babuška, V., 1968. Elastic anisotropy of igneous and metamorphic rocks. Stud. Geophys. Et. Geod. 12 (3), 291–303.
Babuška, V., 1972. Elasticity and anisotropy of dunite and bronzitite. J. Geophys. Res. 77 (35), 6955–6965.
Babuška, V., Pros, Z., 1984. Velocity anisotropy in granodiorite and quartzite due to the distribution of microcracks. Geophys. J. Int. 76 (1), 121–127.
Babuška, V., Cara, M., 1991. Seismic anisotropy in the Earth. Kluwer Academic Publishers, Dordrecht.
Babuška, V., Plomerová, J., 1992. The lithosphere in central Europe—seismological and petrological aspects. Tectonophysics 207 (1–2), 141–163.
Babuška, V., Pros, Z., Franke, W., 1977. Effect of fabric and cracks on the elastic anisotropy in granodiorite. Pubis Inst. Geophys. Pol. Acad. Sci. A-6 117, 179–186.
Babuška, V., Fiala, J., Mayson, D.J., Liebermann, R.C., 1978. Elastic properties of eclogite rocks from the Bohemian massif. Stud. Geophys. Et. Geod. 22 (4), 348–361. https://doi.org/10.1007/BF02179277.
Baerheim, R., 1993. Harmonic decomposition of the anisotropic elasticity tensor. Q J. Mech. Appl. Math. 46 (3), 391–418. https://doi.org/10.1093/qjmam/46.3.391.
Bancroft, D., 1940. An electronic interval-timer for laboratory seismometry. Trans. Am. Geophys. Union, Part II 695–696.
Baratoux L., 2004. Petrology, deformation mechanisms, and fabric of metabasites deformed at natural strain and metamorphic gradient. PhD. thesis, Institute of

Petrology and Structural Geology, Faculty of Science, Charles University, Prague, and Laboratoire Dynamique de la Lithosphere, Universite Claude Bernard Lyon.
Berckhemer, H., Rauen, A., Winter, H., Kern, H., Kontny, A., Lienert, M., Soffel, H.C., 1997. Petrophysical properties of the 9–km-deep crustal section at KTB. J. Geophys. Res.: Solid Earth 102 (B8), 18337–18361.
Berg, C.A., 1965. Deformation of fine cracks under high pressure and shear. J. Geophys. Res. 70 (14), 3447–3452.
Birch, F., 1960. The velocity of compressional waves in rocks to 10 kilobars: 1. J. Geophys. Res. 65 (4), 1083–1102.
Birch, F., 1961. The velocity of compressional waves in rocks to 10 kilobars: Part 2. J. Geophys. Res. 66, 2199–2224.
Bona, A., Bucataru, I., Slawinski, M., 2004. Material symmetries of elasticity tensors. Q J. Mech. Appl. Math. 57 (4), 583–598.
Brace, W.F., 1965. Relation of elastic properties of rocks to fabric. J. Geophys. Res. 70 (22), 5657–5667.
Bur, T.R., Thill, R.E., & Hjelmstad, K.E. (1969). *An ultrasonic method for determining the elastic symmetry of materials* (Vol. 7333). US Department of Interior, Bureau of Mines.
Carcione, J.M., 2014 (extended and revised). Wave Fields in Real Media: Theory and Numerical Simulation of Wave Propagation in Anisotropic, Anelastic, Porous and Electromagnetic Media, 3rd edn.,. Elsevier.
Cerveny, V., 1982. Direct and inverse kinematic problems for inhomogeneous anisotropic media – linearization approach. Contr. Geophys. Inst. Slov. Acad. Sci. 13, 127–133.
Cerveny, V., Jech, J., 1982. Linearized solutions of kinematic problems of seismic body waves in inhomogeneous slightly anisotropic media. J. Geophys. 51, 96–104.
Cerveny, V., Psencik, I., 2005. Plane waves in viscoelastic anisotropic media—I. Theory. Geophys. J. Int. 161, 197–212.
Christensen, N.I., 1965. Compressional wave velocities in metamorphic rocks at pressures to 10 kilobars. J. Geophys. Res. 70 (24), 6147–6164.
Christensen, N.I., 1966. Elasticity of ultrabasic rocks. J. Geophys. Res. 71 (24), 5921–5931.
Christensen, N.I., 1974. Compressional wave velocities in possible mantle rocks to pressures of 30 kilobars. J. Geophys. Res. 79, 407–412.
Christensen, N.I., 1979. Compressional wave velocities in rocks at high temperatures and pressures, critical thermal gradients, and crustal low-velocity zones. J. Geophys. Res.: Solid Earth 84 (B12), 6849–6857.
Christensen, N.I., Mooney, W.D., 1995. Seismic velocity structure and composition of the continental crust: a global view. J. Geophys. Res.: Solid Earth 100 (B6), 9761–9788.
Cowin, S.C., Mehrabadi, M.M., 1987. On the identification of material symmetry for anisotropic elastic materials. Q J. Mech. Appl. Math. 40 (4), 451–476. https://doi.org/10.1093/qjmam/40.4.451.
Diner, C., Kochetov, M., Slawinski, M., 2011. On choosing effective symmetry classes for elasticity tensors. Q J. Mech. Appl. Math. 64 (1), 57–74. https://doi.org/10.1093/qjmam/hbq023.
Fountain, D.M., Christensen, N.I., 1989. Composition of the continental crust and upper mantle: a review. Geophys. Framew. Cont. U. S. 172, 711–742.
Freund, D., 1992. Ultrasonic compressional and shear velocities in dry clastic rocks as a function of porosity, clay content, and confining pressure. Geophys. J. Int. 108, 125–135.
Gakewski, D., Psencik, I., 1998. Polarization, phase velocity and NMO velocity of qP waves in arbitrary weakly anisotropic media. Geophysics 63, 1754–1766.
Greenfield, R.J., Graham, E.K., 1996. Application of a simple relation for describing wave velocity as a function of pressure in rocks containing microcracks. J. Geophys. Res. Solid Earth 101, 5643–5652.
Hakala, M., Kuula, H., Hudson, J.A., 2007. Estimating the transversely isotropic elastic intact rock properties for in situ stress measurement data reduction: a case study of the Olkiluoto mica gneiss, Finland. Int. J. Rock. Mech. Min. Sci. 44 (1), 14–46.
Holbrook, W.S., Mooney, W.D., Christensen, N.I., 1992. The seismic velocity structure of the deep continental crust. Cont. Low. crust 23, 1–43.
Hughes, D.S., Maurette, C.G., 1956. Variation of elastic wave velocities in granites with pressure and temperature. Geophysics 21 (2), 277–284.
Hughes, D.S., Maurette, C., 1957. Variation of elastic wave velocities in basic igneous rocks with pressure and temperature. Geophysics 22 (1), 23–31.
Ivankina, T.I., Zel, I.Y., Lokajicek, T., Kern, H., Lobanov, K.V., Zharikov, A.V., 2017. Elastic anisotropy of layered rocks: Ultrasonic measurements of plagioclase-biotite-muscovite (sillimanite) gneiss versus texture-based theoretical predictions (effective media modeling). Tectonophysics 712–713, 82–94.
Ivankina, T.I., Zel, I.Y., Petruzalek, M., Rodkin, M.V., Matveev, M.A., Lokajicek, T., 2020. Elastic anisotropy, permeability, and freeze-thaw cycling of rapakivi granite. Int. J. Rock. Mech. Min. Sci. 136, 104541.
Jackson, I., Fitz Gerald, J.D., Faul, U.H., Tan, B.H., 2002. Grainsize-sensitive seismic wave attenuation in polycrystalline olivine. J. Geophys. Res., Solid Earth 107, 2360. https://doi.org/10.1029/2001JB001225.
Jahns, E., Siegesmund, S., Chlupac, T., 1994. In situ seismic velocities versus laboratory measurements: an example from the KTB. Sci. Drill. 4, 215–226.
Jech, J., 1991. Computation of elastic parameters of anisotropic medium from travel times of quasi-compressional waves. Phys. Earth Planet. Inter. 66 (3–4), 153–159.
Jech, J., Pšenčík, I., 1989. First-order perturbation method for anisotropic media. Geophys. J. Int. 99, 369–376.
Ji, S., Wang, Q., Marcotte, D., Salisbury, M.H., Xu, Z., 2007. P wave velocities, anisotropy and hysteresis in ultrahigh-pressure metamorphic rocks as a function of confining pressure. J. Geophys. Res.: Solid Earth 112 (B9).
Keppler, R., Ullemeyer, K., Behrmann, J.H., Stipp, M., Kurzawski, R.M., Lokajíček, T., 2015. Crystallographic preferred orientations of exhumed subduction channel rocks from the Eclogite Zone of the Tauern Window (Eastern Alps, Austria), and implications on rock elastic anisotropies at great depths. Tectonophysics 647, 89–104.
Keppler, R., Vasin, R., Stipp, M., Lokajícek, T., Petruzálek, M., Froitzheim, N., 2021. Elastic anisotropies of deformed upper crustal rocks in the Alps. Solid Earth 12 (10), 2303–2326.
Kern, H., 1978. The effect of high temperature and high confining pressure on compressional wave velocities in quartz-bearing and quartz-free igneous and metamorphic rocks. Tectonophysics 44 (1–4), 185–203.
Kern, H., Liu, B., Popp, T., 1997. Relationship between anisotropy of P and S wave velocities and anisotropy of attenuation in serpentinite and amphibolite. J. Geophys. Res.: Solid Earth 102 (B2), 3051–3065.
Kern, H., Lokajicek, T., Svitek, T., Wenk, H.R., 2015. Seismic anisotropy of serpentinite from Val Malenco, Italy. J. Geophys. Res.: Solid Earth 120 (6), 4113–4129.
Kern, H., Ivankina, T.I., Nikitin, A.N., Lokajíček, T., Pros, Z., 2008. The effect of oriented microcracks and crystallographic and shape preferred orientation on bulk elastic anisotropy of a foliated biotite gneiss from Outokumpu. Tectonophysics 457 (3–4), 143–149.
Khazanehdari, J., Rutter, E.H., Brodie, K.H., 2000. High-pressure-high-temperature seismic velocity structure of the midcrustal and lower crustal rocks of the Ivrea-Verbano zone and Serie dei Laghi, NW Italy. J. Geophys. Res.: Solid Earth 105 (B6), 13843–13858.
Klíma, K., 1973. The computation of the elastic constants of an anisotropic medium from the velocities of body waves. Stud. Geophys. Et. Geod. 17, 115–122.
Klíma, K., Babuška, V., 1968. A comparison of measured and calculated elastic anisotropies of marble. Stud. Geophys. Et. Geod. 12 (4), 377–384.
Klíma, K., Vaněk, J., Pros, Z., 1964. The attenuation of longitudinal waves in diabase and greywacke under pressures up to 4 kilobars. Stud. Geophys. Et. Geod. 8, 247–254. https://doi.org/10.1007/BF02606825.
Klíma, K., Pros, Z., Pěč, K., 1981. Search for orthorhombic or higher symmetry in rocks. Stud. Geophys. Et. Geod. 25, 245–261.
Klíma, K., Reinhart, J.S., Vaněk, J., Aurberger, M., Pros, Z., 1962. Ultrasonic attenuation of longitudinal waves in solids. J. Geophys. Res. 67, 2078–2080. https://doi.org/10.1029/JZ067i005p02078.
Li, S., Unsworth, M.J., Booker, J.R., Wei, W., Tan, H., Jones, A.G., 2003. Partial melt or aqueous fluid in the mid-crust of Southern Tibet? Constraints from INDEPTH magnetotelluric data. Geophys. J. Int. 153 (2), 289–304.
Lo, T.W., Coyner, K.B., Toksoz, M.N., 1986. Experimental determination of elastic anisotropy of Berea sandstone, Chicopee shale, and Chelmsford granite. Geophysics 51 (1), 164–171.
Lokajíček, T., Klima, K., 2006. A first arrival identification system of acoustic emission (AE) signals by means of a high-order statistics approach. Meas. Sci. Technol. 17 (9), 2461.
Lokajíček, T., Svitek, T., 2015. Laboratory measurement of elastic anisotropy on spherical rock samples by longitudinal and transverse sounding under confining pressure. Ultrasonics 56, 294–302.
Lokajíček, T., Kern, H., Svitek, T., Ivankina, T., 2014. 3D velocity distribution of P-and S-waves in a biotite gneiss, measured in oil as the pressure medium: Comparison with velocity measurements in a multi-anvil pressure apparatus and with texture-based calculated data. Phys. Earth Planet. Inter. 231, 1–15.
Lokajíček, T., Vasin, R., Svitek, T., Petružálek, M., Kotrlý, M., Turková, I., Wenk, H.R., 2021. Intrinsic elastic anisotropy of Westerly granite observed by ultrasound measurements, microstructural investigations, and neutron diffraction. J. Geophys. Res.: Solid Earth 126 (1) e2020JB020878.
Louis, L., David, C., Špaček, P., Wong, T.F., Fortin, J., Song, S.R., 2012. Elastic anisotropy of core samples from the Taiwan Chelungpu Fault Drilling Project (TCDP): direct 3-D measurements and weak anisotropy approximations. Geophys. J. Int. 188 (1), 239–252.
Machek, M., Špaček, P., Ulrich, S., Heidelbach, F., 2007. Origin and orientation of microporosity in eclogites of different microstructure studied by ultrasound and microfabric analysis. Eng. Geol. 89 (3–4), 266–277.
Mainprice, D., Humbert, M., 1994. Methods of calculating petrophysical properties from lattice preferred orientation data. Surv. Geophys. 15, 575–592.
Martínková, M., Pros, Z., Klíma, K., Lokajícek, T., Kotková, J., 2000. Experimentally determined P-wave velocity anisotropy for rocks related to the Western Bohemia seismoactive region. Stud. Geophys. Et. Geod. 44 (4), 581.
Matthies, S., Humbert, M., 1993. 'The realization of the concept of a geometric mean for calculating physical constants of polycrystalline materials', Phys. Stat. Sol. (b) 177, K47- K50.Matthies, S. (2012). GEO-MIX-SELF calculations of the elastic properties of a textured graphite sample at different hydrostatic pressures. J. Appl. Crystallogr. 45 (1), 1–16.
Mavko, G.M., Nur, A., 1978. The effect of nonelliptical cracks on the compressibility of rocks. J. Geophys. Res.: Solid Earth 83 (B9), 4459–4468.
McKenzie, D., 1979. Finite deformation during fluid flow. Geophys. J. Int. 58 (3), 689–715.
Mussett, A.E., Khan, M.A., 2000. Looking into the earth: an introduction to geological geophysics. Cambridge University Press.
Nur, A., Simmons, G., 1969. Stress-induced velocity anisotropy in rock: an experimental study. J. Geophys. Res. 74 (27), 6667–6674.
Petružálek, M., Lokajíček, T., Svitek, T., Jechumtálová, Z., Kolář, P., Šílený, J., 2019. Fracturing of migmatite monitored by acoustic emission and ultrasonic sounding. Rock. Mech. Rock. Eng. 52, 47–59.
Plomerová, J., Achauer, U., Babuška, V., Vecsey, L., BOHEMA Working Group, 2007. Upper mantle beneath the Eger Rift (Central Europe): plume or asthenosphere upwelling? Geophys. J. Int. 169 (2), 675–682.

Přikryl, R., Lokajíček, T., Pros, Z., Klíma, K., 2007. Fabric symmetry of low anisotropic rocks inferred from ultrasonic sounding: Implications for the geomechanical models. Tectonophysics 431 (1–4), 83–96.
Pros, Z., Babuška, V., 1967. A method for investigating the elastic anisotropy on spherical rock samples. Z. für Geophys. 33 (4), 289–291.
Pros, Z., Babuška, V., 1968. An apparatus for investigating the elastic anisotropy on spherical rock samples. Stud. Geophys. Et. Geod. 12 (2), 192–198.
Pros, Z., Podroužková, Z., 1974. Apparatus for investigating the elastic anisotropy on spherical samples at high pressure, Veröff. Zentralinst. Physic Erde 22, 42–47.
Pros, Z., Lokajíček, T., Klíma, K., 1998. Laboratory approach to the study of elastic anisotropy on rock samples. Geodynamics of Lithosphere & Earth's Mantle: Seismic Anisotropy as a Record of the Past and Present Dynamic Processes. Birkhäuser, Basel, pp. 619–629.
Pros, Z., Lokajíček, T., Přikryl, R., Klíma, K., 2003. Direct measurement of 3D elastic anisotropy on rocks from the Ivrea zone (Southern Alps, NW Italy). Tectonophysics 370 (1–4), 31–47.
Pšenčík, I., Vavryčuk, V., 2002. Approximate relation between the ray vector and wave normal in weakly anisotropic media. Stud. Geophys. Et. Geod. 46, 793–807. https://doi.org/10.1023/A:1021189724526.
Pšenčík, I., Růžek, B., Lokajíček, T., Svitek, T., 2018. Determination of rock-sample anisotropy from P-and S-wave traveltime inversion. Geophys. J. Int. 214 (2), 1088–1104.
Rasolofosaon, P.N., Zinszner, B.E., 2002. Comparison between permeability anisotropy and elasticity anisotropy of reservoir rocks. Geophysics 67 (1), 230–240.
Rawling, G.C., Baud, P., Wong, T.F., 2002. Dilatancy, brittle strength, and anisotropy of foliated rocks: experimental deformation and micromechanical modeling. J. Geophys. Res.: Solid Earth 107((B10), ETG-8.
Ribe, N.M., 1992. On the relation between seismic anisotropy and finite strain. J. Geophys. Res.: Solid Earth 97 (B6), 8737–8747.
Rudnick, R.L., Fountain, D.M., 1995. Nature and composition of the continental crust: a lower crustal perspective. Rev. Geophys. 33 (3), 267–309.
Sano, O., Kudo, Y., Mizuta, Y., 1992. Experimental determination of elastic constants of Oshima granite, Barre granite, and Chelmsford granite. J. Geophys. Res.: Solid Earth 97 (B3), 3367–3379.
Sarout, J., Molez, L., Guéguen, Y., Hoteit, N., 2007. Shale dynamic properties and anisotropy under triaxial loading: experimental and theoretical investigations. Phys. Chem. Earth, Parts A/B/C. 32 (8–14), 896–906.
Shea Jr, W.T., Kronenberg, A.K., 1993. Strength and anisotropy of foliated rocks with varied mica contents. J. Struct. Geol. 15 (9–10), 1097–1121.
Siegesmund, S., Vollbrecht, A., Pros, Z., 1993. Fabric changes and their influence on P-wave velocity patterns—examples from a polyphase deformed orthogneiss. Tectonophysics 225 (4), 477–492.
Siegesmund, S., Kruhl, J.H., & Lüschen, E. (1996). The significance of rock fabrics for the geological-interpretation of geophysical anisotropies.
Stanchits, S., Lockner, D.A., Ponomarev, A.V., 2003. Anisotropic changes in P-wave velocity and attenuation during deformation and fluid infiltration of granite. Bull. Seism. Soc. Am. 93 (4), 1803–1822.
Staněk, M., Géraud, Y., Lexa, O., Špaček, P., Ulrich, S., Diraison, M., 2013. Elastic anisotropy and pore space geometry of schlieren granite: Direct 3-D measurements at high confining pressure combined with microfabric analysis. Geophys. J. Int., 194 (1), Artic., 1 https://doi.org/10.1093/gji/ggt053.
Svitek, T., Rudajev, V., & Petružálek, M. (2010). Determination of P–wave arrival time of acoustic events. *Laboratórne štúdium 3D elastickej anizotropie hornín Laboratory study of 3D elastic anisotropy of rocks*.
Svitek, T., Vavryčuk, V., Lokajíček, T., Petružálek, M., 2014. Determination of elastic anisotropy of rocks from P-and S-wave velocities: numerical modelling and lab measurements. Geophys. J. Int. 199 (3), 1682–1697.
Svitek, T., Vavryčuk, V., Lokajíček, T., Petružálek, M., Kern, H., 2017. Effect of pressure on 3D distribution of P-wave velocity and attenuation in antigorite serpentiniteAnisotropic attenuation in serpentinite. Geophysics 82 (4), WA33–WA43.
Thill, R.E., Willard, R.J., Bur, T.R., 1969. Correlation of longitudinal velocity variation with rock fabric. J. Geophys. Res. 74 no. 20, 4897–4909.
Thill, R.E., Bur, T.R., Steckley, R.C., 1973. Velocity anisotropy in dry and saturated rock spheres and its relation to rock fabric (November). In: International Journal of Rock Mechanics and Mining Sciences & Geomechanics Abstracts, Vol. 10. Pergamon, pp. 535–557 (November).
Thomsen, L., 1986. Weak elastic anisotropy. Geophysics 51, 1954–1966.
Ullemeyer, K., Siegesmund, S., Rasolofosaon, P.N., Behrmann, J.H., 2006. Experimental and texture-derived P-wave anisotropy of principal rocks from the TRANSALP traverse: an aid for the interpretation of seismic field data. Tectonophysics 414 (1–4), 97–116.
Ullemeyer, K., Nikolayev, D.I., Christensen, N.I., Behrmann, J.H., 2011. Evaluation of intrinsic velocity—pressure trends from low-pressure P-wave velocity measurements in rocks containing microcracks. Geophys. J. Int. 185 (3), 1312–1320.
Ullemeyer, K., Spalthoff, P., Heinitz, J., Isakov, N.N., Nikitin, A.N., Weber, K., 1998. The SKAT texture diffractometer at the pulsed reactor IBR-2 at Dubna: experimental layout and first measurements. Nucl. Instrum. Methods Phys. Res. Sect. A 412, 80–88.
Vasin, R.N., Kern, H., Lokajíček, T., Svitek, T., Lehmann, E., Mannes, D.C., Wenk, H.R., 2017. Elastic anisotropy of Tambo gneiss from Promontogno, Switzerland: a comparison of crystal orientation and microstructure-based modelling and experimental measurements. Geophys. J. Int. 209 (1), 1–20.
Vavryčuk, V., 2007a. Asymptotic Green's function in homogeneous anisotropic viscoelastic media. Proc. R. Soc. A 463, 2689–2707.
Vavryčuk, V., 2007b. Ray velocity and ray attenuation in homogeneous anisotropic viscoelastic media. Geophysics 72, D119–D127.
Vavryčuk, V., 2015. Determination of parameters of viscoelastic anisotropy from ray velocity and ray attenuation: theory and numerical modeling. Geophysics 80 (3), C59–C71.
Vavryčuk, V., Svitek, T., Lokajíček, T., 2017. Anisotropic attenuation in rocks: Theory, modelling and lab measurements. Geophys. J. Int. 208 (3), 1724–1739.
Vickers, Byron L., Richard, E.Thill, 1969. A new technique for preparing rock spheres. J. Phys. E: Sci. Instrum. 2 (10), 901.
Walsh, J.B., 1965. The effect of cracks on the compressibility of rock. J. Geophys. Res. 70 (2), 381–389.
Wang, J., Mao, Z., Jiang, F., Duffy, T.S., 2015. Elasticity of single-crystal quartz to 10 GPa. Phys. Chem. Miner. 42, 203–212.
Weiss, T., Rasolofosaon, P.N.J., Siegesmund, S., 2002. Ultrasonic wave velocities as a diagnostic tool for the quality assessment of marble. Geological Society. Special Publications, London, pp. 149–164.
Weiss, T., Siegesmund, S., Rabbel, W., Bohlen, T., Pohl, M., 1999. Seismic velocities and anisotropy of the lower continental crust: a review. Seism. Explor. Deep Cont. crust: Methods Concepts DEKORP Acco. Proj. 97–122.
Wenk, H.R., Matthies, S., Donovan, J., Chateigner, D., 1998. BEARTEX: a Windows-based program system for quantitative texture analysis. J. Appl. Crystallogr. 31, 269–362.
Wenk, H.-R., Lutterotti, L., Vogel, S., 2003. Texture analysis with the new HIPPO TOF diffractometer. Nucl. Instrum. Methods A515, 575–588.
Zang, A., Berckhemer, H., Lienert, M., 1996. Crack closure pressures inferred from ultrasonic drill-core measurements to 8 km depth in the KTB wells. Geophys. J. Int. 124 (3), 657–674.
Zel, I.Y., Petružálek, M., Lokajíček, T., Ivankina, T.I., Kichanov, S.E., Kozlenko, D.P., Duliu, O.G., 2021. Assessment of structural, magnetic, and P-wave velocity anisotropy of two biotite gneisses from X-ray and neutron tomography. Tectonophysics 812, 228925.
Zhu, Y., Tsvankin, I., 2006. Plane-wave propagation in attenuative transversely isotropic media. Geophysics 71 (2), T17–T30.
Zou, W.N., Tang, C.X., Lee, W.H., 2013. Identification of symmetry type of linear elastic stiffness tensor in an arbitrarily orientated coordinate system. Int. J. Solid Struct. 50 (14–15), 2457–2467. https://doi.org/10.1016/j.ijsolstr.2013.03.037.